Available online at www.sciencedirect.com
ScienceDirect
International Journal of Heat and Mass Transfer 51 (2008) 1838–1853
International Journal of HEAT and MASS TRANSFER
www.elsevier.com/locate/ijhmt

Forced convection heat transfer from an elliptical cylinder to power-law fluids

R.P. Bharti [1], P. Sivakumar, R.P. Chhabra *

Department of Chemical Engineering, Indian Institute of Technology, Kanpur 208 016, India

Received 21 February 2007; received in revised form 6 June 2007
Available online 4 September 2007

Abstract

Forced convection heat transfer to incompressible power-law fluids from a heated elliptical cylinder in the steady, laminar cross-flow regime has been studied numerically. In particular, the effects of the power-law index ($0.2 \leqslant n \leqslant 1.8$), Reynolds number ($0.01 \leqslant Re \leqslant 40$), Prandtl number ($1 \leqslant Pr \leqslant 100$) and the aspect ratio of the elliptic cylinder ($0.2 \leqslant E \leqslant 5$) on the average Nusselt number (Nu) have been studied. The average Nusselt number for an elliptic cylinder shows a dependence on the Reynolds and Prandtl numbers and power-law index, which is qualitatively similar to that for a circular cylinder. Thus, heat transfer is facilitated by the shear-thinning tendency of the fluid, while it is generally impeded in shear-thickening fluids. The average Nusselt number values have also been interpreted in terms of the usual Colburn heat transfer factor (j). The functional dependence of the average Nusselt number on the dimensionless parameters (Re, n, Pr, E) has been presented by empirically fitting the numerical results for their easy use in process design calculations.

Keywords: Power-law fluids; Elliptical cylinder; Nusselt number; Reynolds number; Prandtl number; Shear-thinning; Shear-thickening

1. Introduction

Owing to their wide ranging applications, considerable research efforts have been devoted to the steady cross-flow of and heat transfer from cylinders of circular and non-circular cross-sections to Newtonian and non-Newtonian fluids. Typical examples include the flow in tubular and pin heat exchangers, hot wire anemometry, sensors and probes, in the RTM process of manufacturing fiber reinforced composites, in filtration screens and aerosol filters, etc. In addition, this flow also represents a classical flow problem in the domain of transport phenomena. Consequently, a voluminous body of information is now available on various aspects of the flow phenomena associated with the transverse flow of Newtonian fluids over a circular cylinder, e.g., see the extensive reviews available in the literature [1–6]. Suffice it to say that adequate information is now available on most aspects of flow and heat transfer for the flow of Newtonian fluids past a circular cylinder. However, it is fair to say that the flow phenomenon has been studied much more extensively than the corresponding heat/mass transfer problems, even for the flow of Newtonian fluids over a circular cylinder.

On the other hand, it is readily acknowledged that many substances of multi-phase nature and/or of high molecular weight encountered in industrial practice (pulp and paper suspensions, food, polymer melts, solutions and in biological process engineering applications, etc.) display shear-thinning and/or shear-thickening behaviour [7]. Owing to their high viscosity levels, these materials are generally processed in laminar flow conditions. Admittedly, many non-Newtonian fluids, notably polymeric systems display viscoelastic behaviour; the available scant literature both for the creeping flow past a single cylinder and over a periodic array of cylinders seems to suggest the viscoelastic effects to be minor in this flow configuration, at least as far as the gross engineering parameters (drag and heat

* Corresponding author. Tel.: +91 512 259 7393; fax: +91 512 259 0104.
E-mail address: chhabra@iitk.ac.in (R.P. Chhabra).
[1] Present address: Department of Chemical and Biomolecular Engineering, The University of Melbourne, Parkville 3010, Victoria, Australia

0017-9310/$ - see front matter © 2007 Elsevier Ltd. All rights reserved.
doi:10.1016/j.ijheatmasstransfer.2007.06.032

Nomenclature

a	semi-axis of the elliptical cylinder normal to the direction of flow, m
b	semi-axis of the elliptical cylinder along the direction of flow, m
c_p	specific heat of the fluid, J/kg K
E	aspect ratio of the elliptical cylinder, $=b/a$, dimensionless
I_2	second invariant of the rate of the strain tensor, s^{-2}
h	local convective heat transfer coefficient, W/m^2 K
j	Colburn factor for heat transfer, dimensionless
k	thermal conductivity of the fluid, W/m K
m	power-law consistency index, Pa s^n
n	power-law flow behaviour index, dimensionless
$Nu(\theta)$	local Nusselt number, dimensionless
Nu	average Nusselt number, dimensionless
P	pressure, Pa
Pr	Prandtl number, dimensionless
Re	Reynolds number, dimensionless
U_∞	uniform inlet velocity of the fluid, m/s
T	temperature, K
T_∞	temperature of the fluid at the inlet, K
T_w	temperature at the surface of the cylinder, K
U_x, U_y	x- and y-components of the velocity, m/s
x, y	stream-wise and transverse coordinates, m
X_N	normalized average Nusselt number using the corresponding Newtonian value, dimensionless
X_E	normalized average Nusselt number using the corresponding value for circular cylinder, dimensionless

Greek symbols

η	viscosity, Pa s
θ	angular displacement from the front stagnation ($\theta = 0$), degrees
ρ	density of the fluid, kg/m^3
τ	extra stress, Pa

transfer characteristics) are concerned [4]. Therefore, it seems reasonable to begin the analysis with the flow of purely viscous power-law type fluids and the level of complexity can gradually be built up to accommodate the other non-Newtonian characteristics.

As far as known to us, there has been no prior study on the forced convection heat transfer in power-law fluids from an elliptical cylinder. This constitutes the main objective of this work. At the outset, it is desirable, however, to briefly recount the available limited work on the flow of Newtonian and power-law fluids past an elliptical cylinder to facilitate the subsequent presentation of the new results for the forced convection heat transfer in power-law fluids from an elliptical cylinder.

2. Previous work

As noted earlier, while the fluid mechanical aspects of the flow of Newtonian fluids over a circular cylinder have been thoroughly reviewed elsewhere, the corresponding heat transfer literature has been summarized recently by Bharti et al. [8]. In contrast, only limited information is available even for the Newtonian fluid flow over an elliptical cylinder [9].

Even less is known about the power-law fluid flow and heat transfer from a circular cylinder in the steady cross-flow regime. The available literature comprises four creeping flow studies [10–13] and suffice it to say here that all of these analyses are internally consistent with each other. Similarly, only a few studies are available in the steady cross-flow regime relating to finite values of the Reynolds number [9,14–23]. The limits of the cessation of the creeping flow regime and transition from 2D steady symmetric flow to asymmetric flow regimes have been delineated only recently [21] for the flow of power-law fluids across a circular cylinder. This study showed that shear-thickening fluid behaviour can advance the formation of asymmetric wakes. All in all, reliable results are now available for the flow of power-law fluid over a circular cylinder in the two-dimensional steady symmetric flow regime embracing the range of conditions as: $Re \leqslant 40$; $0.2 \leqslant n \leqslant 2$. On the other hand, there have been only three studies [15,17,23] on forced convection heat transfer from a circular cylinder in the steady cross-flow regime. In addition to the local and global heat transfer characteristics, these authors also presented the dependence of the heat transfer on the thermal boundary conditions imposed at the surface of the cylinder. Combined together, these studies encompass the ranges of Reynolds number as $5 \leqslant Re \leqslant 40$, of power-law index $0.6 \leqslant n \leqslant 2$ and Prandtl number as $1 \leqslant Pr \leqslant 100$ and for the two commonly used thermal boundary conditions (i.e., isothermal and isoflux) on the surface of the cylinder. These numerical results have been correlated using simple predictive expressions to permit an easy estimation of the value of the average heat transfer coefficient for a cylinder immersed in streaming power-law liquids. The available scant experimental studies have also been summarized elsewhere [2–4,24] and these are not repeated here. Suffice it to add here that the preliminary comparisons between the predictions and the scant mass transfer results are encouraging.

In contrast, as far as known to us, there has only one study dealing with the steady flow of power-law fluids over an elliptical cylinder [9]. Extensive results were presented on the individual and total drag coefficients, streamline and surface pressure profiles and their functional dependence

on the pertinent dimensionless parameters over the ranges as: Reynolds number in the range $0.01 \leqslant Re \leqslant 40$, power-law index as $0.2 \leqslant n \leqslant 1.9$ and the aspect ratio of the elliptical cylinder as $0.2 \leqslant E \leqslant 5$. The only other relevant work is that of Woods et al. [25] who studied the creeping flow of power-law fluids in periodic arrays of elliptic cylinders. In principle, in the limit of vanishingly small volume fraction of solid, these results should approach that for a single elliptic cylinder. In practice, however, owing to the highly non-linear relationship between drag and solid volume fraction, this extrapolation step necessitates the knowledge of such results for very small values of the solid volume fraction in order to extract the results for a single cylinder using this approach. Since the detailed discussion of the available literature on the Newtonian flow past an unconfined elliptic cylinder has been presented elsewhere [9], these details are not repeated here. On the other hand, only limited results are available on heat transfer even in Newtonian fluids from elliptical cylinder. For instance, Chao and Fagbenle [26] presented a boundary layer solution for the forced convection heat transfer from elliptical cylinder in cross-flow using the Merk's and the Blasius–Frossling method. More recently, another boundary layer analysis based on the application of the well-known Von Karman–Pohlhausen integral method has been carried out by Khan et al. [27]. However, their analysis not only implicitly assumes large values of the Prandtl number (thin thermal boundary layer), but is also limited to elliptic cylinders with $E \geqslant 1$. A numerical solution of the two-dimensional Navier–Stokes and energy equations for forced convection heat transfer from an elliptic cylinder was reported by D'Alessio and Dennis [28] for two values of the Reynolds number of 5 and 20 and for Prandtl numbers ranging from 1 to 25. They presented correlations for the average Nusselt number in terms of the Peclet number for three different angles of inclinations (30°, 40° and 70°). Badr [29,30] has numerically investigated the two-dimensional laminar forced and mixed convection heat transfer from an isothermal elliptic cylinder to air ($Pr = 0.7$). He reported the influence of Reynolds number (20–500), angle of inclination (0–90°) and aspect ratio (0.4–0.9) on heat transfer. The effect of fluctuations in the free-stream velocity on the mixed convection heat transfer from an elliptic cylinder has been studied by Ahmad and Badr [31] for three values of the Reynolds numbers of 50, 100 and 150 and Grashof numbers as 20,000, 30,000 and 50,000.

Admittedly, scant experimental results are also available for the flow and heat transfer from elliptic cylinders (e.g., see [32–34], etc.), but most of these have focused on the unsteady (high Reynolds number) flow characteristics and are thus not of direct relevance to the present work.

In summary, thus, as far as known to us, there has been no prior study dealing with the forced convection heat transfer from an elliptical cylinder to power-law fluids. This work is concerned with the investigation of the two-dimensional forced convection heat transfer in incompressible power-law fluids from an isothermal cylinder of elliptical cross-section over the following ranges of the Reynolds number ($0.01 \leqslant Re \leqslant 40$), Prandtl number ($0.7 \leqslant Pr \leqslant 100$), the power-law index ($0.2 \leqslant n \leqslant 1.8$) and for aspect ratio ($0.2 \leqslant E \leqslant 5$).

3. Problem statement and governing equations

Consider the two-dimensional, laminar, steady flow of an incompressible power-law liquid with a uniform velocity and temperature (U_∞, T_∞) across an infinitely long cylinder of elliptical cross-section (aspect ratio, E). The surface of the cylinder is maintained at a constant temperature, $T_w (> T_\infty)$. Both, the thermo-physical properties of the streaming liquid are assumed to be independent of the temperature and the viscous dissipation effects are neglected. These two assumptions lead to the de-coupling of the momentum and the thermal energy equations, but at the same time restrict the applicability of these results to the situations where the temperature difference is not too great and for moderate viscosity and/or shearing levels. The temperature difference between the surface of the cylinder and the streaming liquid $\Delta T (= T_w - T_\infty)$ is assumed to be small (≈ 2 K) so that the variation of the physical properties, notably, density and viscosity, with temperature could be neglected. Also, the unconfined flow condition is simulated here by enclosing an isothermal elliptic cylinder in a circular outer boundary (of diameter D_∞), as shown schematically in Fig. 1. The diameter of the outer circular boundary D_∞ is taken to be sufficiently large to minimize the boundary effects (Fig. 1).

The continuity, momentum and thermal energy equations for this flow problem in their compact forms are written as follows:

- Continuity equation:

$$\nabla \cdot U = 0 \tag{1}$$

- Momentum equation:

$$\rho(U \cdot \nabla U - f) - \nabla \cdot \sigma = 0 \tag{2}$$

- Thermal energy equation:

$$\rho c_p (U \cdot \nabla T) - k \nabla^2 T = 0 \tag{3}$$

where ρ, U, T, f and σ are the density, velocity (U_x and U_y components in Cartesian coordinates), temperature, body force and the stress tensor, respectively. The stress tensor, sum of the isotropic pressure, p and the deviatoric stress tensor (τ), is given by

$$\sigma = -pI + \tau \tag{4}$$

The rheological equation of state for incompressible fluids is given by

$$\tau = 2\eta\varepsilon(U) \tag{5}$$

where $\varepsilon(U)$, the components of the rate of strain tensor, are given by

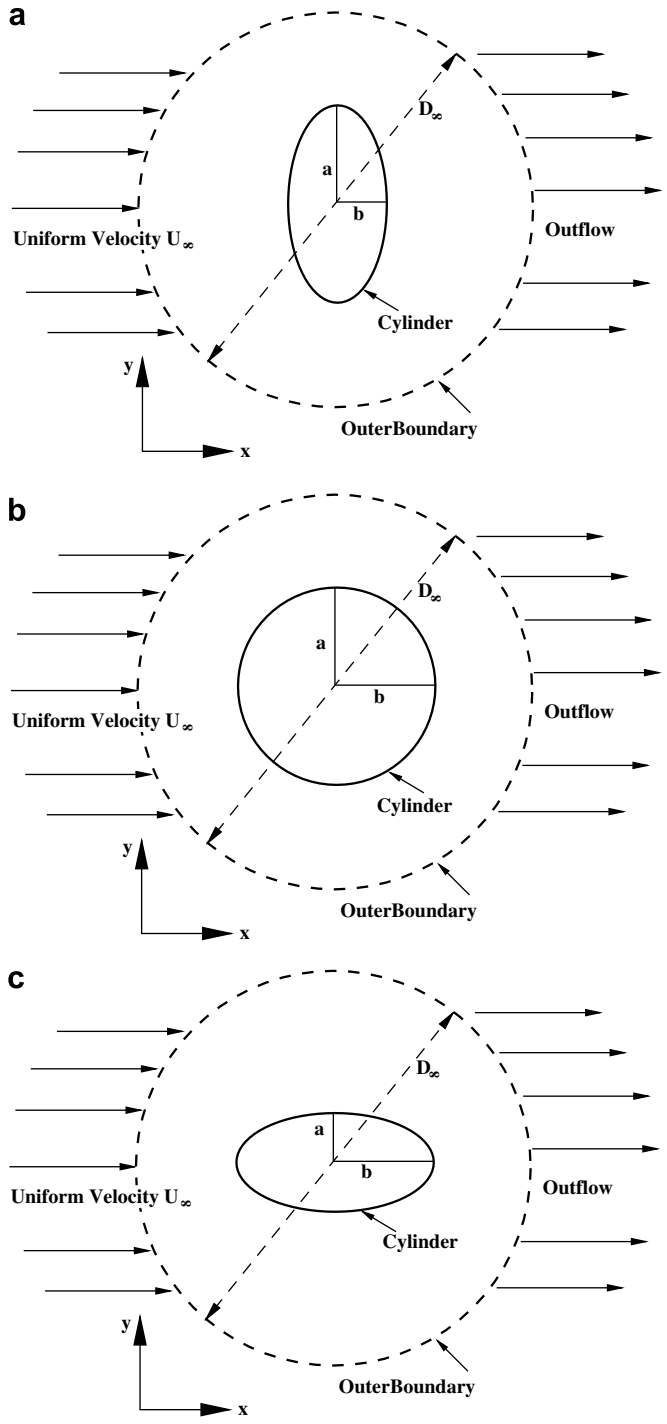

Fig. 1. Schematic representation of the unconfined flow (uniform velocity, U_∞ and free-stream temperature, T_∞) around an isothermal (temperature T_w) elliptical cylinder. (a) $E < 1$ ($a > b$), (b) $E = 1$ ($a = b$, circular cylinder), (c) $E > 1$ ($a < b$).

$$\varepsilon(U) = \frac{(\nabla U) + (\nabla U)^{\mathrm{T}}}{2} \tag{6}$$

For a power-law fluid, the viscosity (η) is given by

$$\eta = m(I_2/2)^{(n-1)/2} \tag{7}$$

where m is the power-law consistency index and n is the power-law index of the fluid ($n < 1$: shear-thinning; $n = 1$: Newtonian; and $n > 1$: shear-thickening fluid) and I_2 is the second invariant of the rate of strain tensor (ε) given by

$$I_2 = 2(\varepsilon_{xx}^2 + \varepsilon_{yy}^2 + \varepsilon_{xy}^2 + \varepsilon_{yx}^2) \tag{8}$$

and the components of the rate of strain tensor are related to the velocity components in Cartesian coordinates as follows:

$$\varepsilon_{xx} = \frac{\partial U_x}{\partial x}; \quad \varepsilon_{yy} = \frac{\partial U_y}{\partial y}; \quad \varepsilon_{xy} = \varepsilon_{yx} = \frac{1}{2}\left(\frac{\partial U_x}{\partial y} + \frac{\partial U_y}{\partial x}\right) \tag{9}$$

The physically realistic boundary conditions for this flow configuration may be written as follows:

- *At the inlet boundary*: The uniform flow condition is imposed at the inlet.

$$U_x = U_\infty, \quad U_y = 0 \quad \text{and} \quad T = T_\infty \tag{10}$$

- *On the surface of the isothermal cylinder*: The standard *no-slip* condition is used, i.e.,

$$U_x = 0, \quad U_y = 0 \quad \text{and} \quad T = T_w \tag{11}$$

- *At the plane of symmetry*, *i.e.*, *center line* ($y = 0$): the symmetric flow condition has been used. It can be written as follows:

$$\frac{\partial U_x}{\partial y} = 0, \quad U_y = 0 \quad \text{and} \quad \frac{\partial T}{\partial y} = 0 \tag{12}$$

- *At the exit boundary*: The default outflow boundary condition option in FLUENT (a zero diffusion flux for all flow variables) was used in this work. In essence, this choice implies that the conditions of the outflow plane are extrapolated from within the domain and as such have negligible influence on the upstream flow conditions. The extrapolation procedure used by FLUENT updates the outflow velocity and the pressure in a manner that is consistent with the fully-developed flow assumption, when there is no area change at the outflow boundary. Note that gradients in the cross-stream direction may still exist at the outflow boundary. Also, the use of this condition obviates the need to prescribe a boundary condition for pressure. This is similar to the homogeneous Neumann condition, given by

$$\frac{\partial U_x}{\partial x} = 0, \quad \frac{\partial U_y}{\partial x} = 0 \quad \text{and} \quad \frac{\partial T}{\partial x} = 0 \tag{13}$$

Owing to the symmetry of the flow over the range of conditions studied herein, the computations have been carried out in the upper half ($y \geqslant 0$) of the computational domain (Fig. 1). The numerical solution of the governing equations (Eqs. (1)–(3)) in conjunction with the above-noted boundary conditions (Eqs. (10)–(13)) yields the primitive variables, i.e., velocity (U_x and U_y), pressure (p) and temperature (T) fields. The flow and thermal fields, in turn, are used to deduce the local and global characteristics like

drag coefficients, stream function, vorticity, surface pressure coefficient, local and average Nusselt number, etc., as described elsewhere [8,9,14–17,21,22]. At this point, it is appropriate to introduce some definitions:

- The Reynolds (Re), and Prandtl (Pr) numbers for power-law fluids are defined as follows:

$$Re = \frac{\rho(2a)^n U_\infty^{2-n}}{m} \quad \text{and} \quad Pr = \frac{c_p m}{k}\left(\frac{U_\infty}{2a}\right)^{n-1}$$

- The values of the *local Nusselt number*, $Nu(\theta)$ on the surface of an isothermal elliptical cylinder are evaluated using the temperature field as follows:

$$Nu(\theta) = \frac{h(2a)}{k} = -\frac{\partial T}{\partial \mathbf{n}_s} \tag{14}$$

where the $\mathbf{n}_s$ (the unit vector normal to the surface of the cylinder) is given as

$$\mathbf{n}_s = \frac{(x/a^2)e_x + (y/b^2)e_y}{\sqrt{\left(\frac{x}{a^2}\right)^2 + \left(\frac{y}{b^2}\right)^2}} = \mathbf{n}_x\mathbf{e}_x + \mathbf{n}_y\mathbf{e}_y$$

where $\mathbf{e}_x$ and $\mathbf{e}_y$ are the x- and y-components of the unit vector, respectively. Such local values are further averaged over the surface of the cylinder to obtain the surface averaged (or overall mean) Nusselt number as follows:

$$Nu = \frac{1}{2\pi}\int_0^{2\pi} Nu(\theta)\mathrm{d}\theta \tag{15}$$

The average Nusselt number (or dimensionless heat transfer coefficient) can be used in process engineering design calculations to estimate the rate of heat transfer from an isothermal cylinder. Dimensional analysis of the field equations and the boundary conditions suggests the average Nusselt number to be a function of the Reynolds and Prandtl numbers, power-law index and the shape of the elliptical cylinder. This relationship is developed in this study.

4. Numerical solution procedure

This numerical investigation has been carried out using FLUENT (version 6.2). The unstructured 'quadrilateral' cells of non-uniform grid spacing were generated using the commercial grid generator GAMBIT. The two-dimensional, steady, laminar, segregated solver was used to solve the incompressible flow on the collocated grid arrangement. The *second order upwind* scheme has been used to discretize the convective terms in the momentum and energy equations. The semi-implicit method for the pressure linked equations (SIMPLE) scheme was used for solving the pressure–velocity decoupling. The '*constant density*' and '*non-Newtonian power-law*' viscosity models were used. FLUENT solves the system of algebraic equations using the Gauss–Siedel (G–S) point-by-point iterative method in conjunction with the algebraic multi-grid (AMG) method solver. The use of AMG scheme can greatly reduce the number of iterations and thus, CPU time required to obtain a converged solution, particularly when the model contains a large number of control volumes. Relative convergence criteria of 10^{-10} for the continuity and x- and y-components of the velocity and of 10^{-15} for temperature were used in this work.

5. Choice of numerical parameters

Needless to say that the reliability and accuracy of the numerical results is contingent upon a prudent choice of the numerical parameters, namely, an optimal domain and grid size. It is, obviously, not possible to simulate truly unconfined flow in such numerical studies. In this study, the domain is characterized by the diameter (D_∞) of the faraway cylindrical envelope of fluid. An excessively large value of D_∞ will warrant enormous computational resources and a small value will unduly influence the results and hence a judicious choice is vital to the accuracy of the results. Similarly, an optimal grid size should meet two conflicting requirements, namely, it should be fine enough to capture the flow field especially near the cylinder yet it should not be exorbitantly resources intensive. The effects of these parameters (D_∞ and grid size) on the drag coefficient values for the power-law fluid flow past an unconfined elliptical cylinder have been assessed extensively recently [9], only the additional results showing the influence of these parameters on the average Nusselt number are presented here thereby ensuring the present results to be free from these artifacts.

5.1. Domain independence study

Following our recent study [9], several values of $D_\infty/2a$ ranging from 100 to 1200 have been used in this study to examine the role of domain size on the heat transfer results.

Table 1 shows the effect of domain size ($D_\infty/2a$) on the average Nusselt number (Nu) for three values of the power-law index ($n = 0.2$, 1 and 1.8), three values of the Reynolds number ($Re = 0.01$, 5 and 40) and for extreme values of the aspect ratio ($E = 0.2$ and 5) at the highest value of the Prandtl number ($Pr = 100$) considered in this work. It can be seen that at $n = 1$ and $Re = 0.01$, an increase in the domain size from 1000 to 1200 alters the average Nusselt number values by 0.22% and 0.68% for $E = 0.2$ and 5, respectively. The corresponding changes for $Re = 0.01$ and $E = 0.2$ are seen to be 0.008% and 0.034% as the domain size is varied from 700 to 900; similarly, for an increase in the value of ($D_\infty/2a$) from 900 to 1200 for $E = 5$ at $n = 0.2$ and 1.8, respectively, alters the values of the Nusselt number by 0.02% and 0.07%. Furthermore, the change in the domain size from 200 to 300 and 250 to 300 for $Re = 5$ and 40 is found to yield very small change in the average Nusselt number values (maximum change being 0.1% and 0.15%

Table 1
Domain independence study for heat transfer from an unconfined elliptical cylinder

Domain size $D_\infty/(2a)$	Re	Average Nusselt number (Nu at $Pr = 100$)					
		Aspect ratio, $E = 0.2$			Aspect ratio, $E = 5$		
		$n = 0.2$	$n = 1$	$n = 1.8$	$n = 0.2$	$n = 1$	$n = 1.8$
500	0.01	1.3125	–	–	0.5167	–	–
700		1.3124	0.9335	0.8812	0.5168	0.3146	0.3016
900		–	0.9270	0.8803	–	0.3110	0.3010
1000		–	0.9245	0.8800	–	0.3097	0.3008
1200		1.3123	0.9265	–	0.5169	0.3076	–
100	5	0.9394	6.5393	6.1379	6.3429	–	3.3968
200		0.9396	6.5205	6.1209	3.3430	3.6410	3.3846
300		0.9396	6.5144	6.1156	6.3427	3.6355	3.3808
250	40	31.7771	21.1045	18.1773	11.5821	9.4144	8.2192
300		31.7735	21.0982	18.1746	11.5826	9.4091	8.2148

for $E = 0.2$ and 5, respectively) for $n = 0.2$, 1 and 1.8. It needs to be emphasized here that the extremely small changes seen in the values of the Nusselt number are accompanied by a 2–3 fold increase in CPU times for the extreme conditions. These results also reinforce two points: firstly, owing to the slow decay of the velocity field, much larger domain is needed to approximate the unconfined flow condition at low Reynolds numbers than that at high Reynolds numbers. Secondly, all else being equal, it appears that the flow field decays much faster in power-law fluids than that in Newtonian fluids and it is therefore possible to work with somewhat shorter domains. This is a distinct advantage, at least at low Reynolds numbers.

Thus, keeping in mind these two conflicting requirements, the domain size of 1200 and 300 are believed to be adequate in the Reynolds number range of $0.01 \leqslant Re \leqslant 5$ and $5 \leqslant Re \leqslant 40$, respectively, over the power-law index range ($0.2 \leqslant n \leqslant 1.8$) considered here, to obtain the results which are believed to be essentially free from domain effects.

5.2. Grid independence study

Having fixed the domain size, the grid independence study has been carried out by using three non-uniform unstructured grids (G1, G2 and G3 with details as shown in Table 2) for the two extreme values of the Reynolds number ($Re = 0.01$ and 40), for the highest value of the Prandtl number ($Pr = 100$) used in this study, for three values of the power-law index ($n = 0.2$, 1 and 1.8) and for extreme values of the aspect ratio, i.e., $E = 0.2$ and 5. Since their relative effects on the fluid-dynamic drag have already been reported elsewhere [9], the additional sensitivity analysis for the average Nusselt number (Nu) is presented here (Table 2). It can be seen from these results that, in moving from grid G2 to G3, the maximum change in the average Nusselt number values is 0.22% and 0.08% at $Re = 40$ for $E = 0.2$ and 5, respectively, for $n = 0.2$, 1 and 1.8. The corresponding changes at $Re = 0.01$ are seen to be 0.08% and 0.02% for $E = 0.2$ and 5, respectively. In view of these negligible changes (accompanied by up to 2–3 fold increase in

Table 2
Grid independence study for heat transfer from an unconfined elliptical cylinder

Grid details				Re	Average Nusselt number (Nu at $Pr = 100$)		
Grid	N_{cells}	N_c	$\delta/(2a)$		$n = 0.2$	$n = 1$	$n = 1.8$
Aspect ratio, $E = 0.2$							
G1	10,000	100	0.0100	40	34.7404	22.9639	19.2179
G2	24,000	200	0.0018		31.6049	21.1445	18.1866
G3	30,000	200	0.013		31.5369	21.0994	18.1635
G2	1,07,800	200	0.0018	0.01	1.3125	0.9925	0.8863
G3	1,28,000	200	0.0010		1.3120	0.9248	0.8851
Aspect ratio, $E = 5$							
G1	16,000	100	0.0070	40	15.4554	9.4046	8.2228
G2	20,000	200	0.0015		16.1907	9.4328	8.2348
G3	33,600	240	0.0010		16.2041	9.4375	8.2385
G2	61,200	200	0.0015	0.01	0.5168	0.3076	0.3006
G3	65,200	240	0.0010		0.5169	0.3076	0.3006

N_{cells} is the number of quadrilateral cells in the computational domain; N_c is the number of points on the surface of the half cylinder and $\delta/(2a)$ is the grid spacing in the vicinity of the cylinder.

the computational time), the grid G2 is considered to be sufficient to resolve the flow and heat transfer phenomena with acceptable levels of accuracy within the range of conditions of interest here. Finally, to add further weight to our claim for the accuracy of the results, the numerical results obtained herein have been compared with the literature values in the next section.

6. Results and discussion

In this work, the fully converged velocity field [9] was used as the input to the thermal energy equation. The two-dimensional steady computations have been carried out for the following values of the dimensionless parameters: Reynolds number, $Re = 0.01$, 0.1, 1, 10, 20 and 40; the power-law index, $n = 0.2$, 0.6, 1, 1.4, and 1.8 thereby covering both shear-thinning ($n < 1$) and shear-thickening ($n > 1$) fluids, Prandtl number, $Pr = 1$, 10, 50 and 100, and for five values of the aspect ratio of the elliptical cylinder, $E = 0.2$, 0.5, 1, 2 and 5. The flow of Newtonian fluids is known to be two-dimensional and steady with or without two symmetric vortices over this range of Reynolds number [5,33–39] and this is assumed to be so for power-law fluids also. Owing to the flow symmetry, the results have been obtained using the half domain ($y \geqslant 0$ in Fig. 1) of the computational domain. However, prior to presenting the new results, it is appropriate to validate the solution procedure to ascertain the accuracy and reliability of the heat transfer results presented herein.

6.1. Validation of results

Since extensive validations for the flow of Newtonian and power-law fluids over circular and elliptical cylinders and of heat transfer results from a circular cylinder have been reported previously [8,9,14–17,21,22], only the additional comparisons for heat transfer from an elliptical cylinder to Newtonian and from circular cylinder to power-law fluids are reported herein. Table 3 compares the average Nusselt number (Nu) values for heat transfer in Newtonian fluids (air) from an elliptical cylinder ($E = 1$, 2 and 5) for various values of the Reynolds number ($0.01 \leqslant Re \leqslant 40$) with the literature values. An excellent correspondence can be seen to exist between the present and literature values for Newtonian fluids; the maximum difference being of the order of ~3%.

Table 4 shows a similar comparison for heat transfer from a circular cylinder to power-law liquids. Once again, the present results can be seen in close agreement (<5%) with the literature results. It needs to be emphasized here that owing to the non-linear viscous terms, the results for power-law liquids are expected to be intrinsically less accurate than that for Newtonian fluids. Inspite of this, the deviations of this order as that seen in Tables 3 and 4 are not uncommon in such numerical studies and may be attributed to different numerics and solvers, domain, grid, etc. used by different investigators. In summary, based on our previous experience coupled with the fact that the numerical predictions for power-law fluids tend to be less accurate, the present results are believed to be reliable to within $\pm 2 - 3\%$.

6.2. Heat transfer results

Dimensional considerations suggest the Nusselt number to be a function of the Reynolds number (Re), flow behaviour index (n), Prandtl number (Pr) and the aspect ratio (E). This relationship is explored in this section. The average Nusselt number values have also been interpreted in terms of the Colburn heat transfer factor, j.

6.2.1. Average Nusselt number (Nu)

The dependence of the average Nusselt number (Nu) on the Reynolds number (Re), power-law index (n), Prandtl number (Pr) is shown in Tables 5–7 for the elliptical cylinder of the aspect ratio of $E < 1$, $E = 1$ and $E > 1$, respectively. Form these tables, it can seen that irrespective of the shape (E) of the cylinder, the average Nusselt number (Nu) shows a dependence on the Reynolds and Prandtl numbers and power-law index, which is qualitatively similar to that for a circular cylinder. For a fixed value of the Reynolds number, the average Nusselt number increases

Table 3
Comparison of the average Nusselt number (Nu) for heat transfer in Newtonian fluids (air) from an unconfined elliptical cylinder

Source	$Re = 0.01$	$Re = 0.1$	$Re = 20$	$Re = 40$
E = 1				
Present results	0.3054	0.4481	2.4500	3.2622
Dennis et al. [40]	0.3020	0.4520	2.5570	3.4800
Lange et al. [41]	0.2900	0.4400	2.4087	3.2805
Mettu et al. [42]	0.3080	0.4530	2.5400	3.3370
Bharti et al. [8]	–	–	2.4653	3.2825
	$Re = 20$	$Re = 50$	$Re = 20$	
E = 2			*E = 5*	
Present results	3.1072	4.6118	2.7338	
Badr [28]	3.0000	4.4900	2.8100	

Table 4
Comparison of the average Nusselt number (Nu) for heat transfer in power-law liquids ($Pr = 1$) from an unconfined circular cylinder ($E = 1$)

Re	Source	$n = 0.8$	$n = 1$	$n = 1.2$	$n = 1.4$
5	Present results	1.5992	1.5641	1.5396	1.5217
	Bharti et al. [15]	1.6844	1.5855	1.5317	1.5011
	Soares et al. [23]	1.6214	1.5896	1.5662	1.5481
10	Present results	2.1234	2.0597	2.0110	1.9727
	Bharti et al. [15]	2.2274	2.0874	2.0020	1.9475
	Soares et al. [23]	2.1164	2.0577	2.0111	1.9730
40	Present results	3.8296	3.6533	3.4132	3.4003
	Bharti et al. [15]	3.9915	3.7030	3.3522	3.3522
	Soares et al. [23]	3.7359	3.5695	3.3249	3.3249

Table 5
Variation of the Average Nusselt number (Nu) for heat transfer in non-Newtonian power-law liquids from an unconfined elliptical ($E < 1$) cylinder with Reynolds and Prandtl numbers and power-law index

n	$Re = 0.01$	$Re = 0.1$	$Re = 1$	$Re = 10$	$Re = 40$	$Re = 0.01$	$Re = 0.1$	$Re = 1$	$Re = 10$	$Re = 40$
Pr = 1, E = 0.2						*Pr = 1, E = 0.5*				
0.2	0.4520	0.6909	1.3120	2.8103	4.6045	0.4057	0.6316	1.2478	2.8452	4.8899
0.6	0.4501	0.6666	1.1408	2.4518	4.2649	0.4039	0.6077	1.0725	2.4383	4.3411
1	0.4411	0.6374	1.0959	2.3130	3.9791	0.3950	0.5797	1.0274	2.2843	3.9727
1.4	0.4423	0.6435	1.0936	2.2260	3.7594	0.3964	0.5858	1.0255	2.1906	3.7222
1.8	0.4463	0.6521	1.0985	2.1672	3.5988	0.4002	0.5940	1.0309	2.1286	3.5495
Pr = 10, E = 0.2						*Pr = 10, E = 0.5*				
0.2	0.6909	1.3123	2.7147	6.2272	12.1432	0.6316	1.2482	2.7533	6.6355	12.7234
0.6	0.6664	1.1179	2.1006	4.9273	10.3427	0.6076	1.0489	2.0689	5.1293	10.2926
1	0.6117	0.9833	1.9198	4.4836	9.2555	0.5543	0.9146	1.8704	4.5780	9.0300
1.4	0.6030	0.9717	1.8725	4.2471	8.5864	0.5469	0.9039	1.8203	4.2783	8.3233
1.8	0.6178	0.9868	1.8584	4.1103	8.1610	0.5613	0.9194	1.8067	4.1054	7.8988
Pr = 50, E = 0.2						*Pr = 50, E = 0.5*				
0.2	1.0580	2.1874	4.4192	10.9178	23.6322	0.9915	2.1711	4.7635	11.9860	24.7283
0.6	0.9447	1.6964	3.2809	8.1228	18.6956	0.8774	1.6401	3.3710	8.6205	18.4188
1	0.8090	1.4088	2.9347	7.4689	16.4384	0.7427	1.3408	2.9537	7.5361	15.8714
1.4	0.7740	1.3593	2.8257	7.1729	15.1327	0.7103	1.2916	2.8283	7.0902	14.5466
1.8	0.7892	1.3677	2.7786	7.0112	14.3377	0.7256	1.3012	2.7783	6.8907	13.7870
Pr = 100, E = 0.2						*Pr = 100, E = 0.5*				
0.2	1.3125	2.7068	5.4419	13.9458	31.4441	1.2482	2.7470	6.0454	15.4563	32.7558
0.6	1.1174	2.0452	3.9886	10.1959	24.1745	1.0484	2.0085	4.1804	10.7913	23.7071
1	0.9266	1.6660	3.5478	9.4380	21.1617	0.8569	1.6043	3.6246	9.4255	20.3383
1.4	0.8733	1.5928	3.4014	9.0659	19.4235	0.8067	1.5295	3.4505	8.9343	18.6051
1.8	0.8865	1.5961	3.3323	8.8661	18.3678	0.8203	1.5342	3.3749	8.7015	17.6189

Table 6
Variation of the Average Nusselt number (Nu) for heat transfer in non-Newtonian power-law liquids from an unconfined elliptical ($E = 1$) cylinder with Reynolds and Prandtl numbers and power-law index

n	$Re = 0.01$	$Re = 0.1$	$Re = 1$	$Re = 10$	$Re = 40$
Pr = 1					
0.2	0.3276	0.5231	1.0847	2.6303	4.7623
0.6	0.3259	0.5009	0.9190	2.2117	4.0545
1	0.3189	0.4767	0.8781	2.0597	3.6534
1.4	0.3200	0.4821	0.8771	1.9727	3.4004
1.8	0.3230	0.4895	0.8830	1.9165	3.2321
Pr = 10					
0.2	0.5231	1.0851	2.5434	6.4244	12.0884
0.6	0.5007	0.8959	1.8586	4.8231	9.2910
1	0.4550	0.7742	1.6639	4.2621	8.0576
1.4	0.4487	0.7654	1.6178	3.9629	7.4086
1.8	0.4608	0.7803	1.6078	3.7848	7.0314
Pr = 50					
0.2	0.8480	1.9662	4.6340	11.8579	22.9364
0.6	0.7402	1.4464	3.1304	8.2622	16.3920
1	0.6205	1.1649	2.6990	7.1136	13.9963
1.4	0.5921	1.1211	2.5777	6.5418	12.8266
1.8	0.6055	1.1319	2.5350	6.2767	12.1804
Pr = 100					
0.2	1.0851	2.5392	6.0091	15.3661	30.0033
0.6	0.8953	1.7975	3.9324	10.4122	20.8647
1	0.7227	1.4106	3.3471	8.8867	17.7713
1.4	0.6782	1.3426	3.1763	8.1755	16.2899
1.8	0.6904	1.3495	3.1112	7.8971	15.4865

with the increasing Prandtl number, irrespective of the fluid behaviour and of the shape of the cylinder. A stronger dependence of the Prandtl number can be seen in shear-thinning ($n < 1$) fluids thereby implying that shear-thinning behaviour promotes heat transfer. In contrast, the shear-thickening ($n > 1$) fluids show not only a somewhat weaker but also an opposite type of dependence. For a fixed value of the flow behaviour index (n), the average Nusselt number increases with the Prandtl number and/or the Reynolds number and/or both. For fixed values of the Reynolds and Prandtl numbers and power-law index, the decreasing value of the aspect ratio (E) enhances the rate of heat transfer, i.e., increases the value of the average Nusselt number. This is so presumably due to the sharp bending of isotherms due to the increasing non-streamlining of the cylinder [9].

The functional dependence of the average Nusselt number (Nu) on the pertinent dimensionless parameters (Re, Pr, n, E) over the range of conditions considered here ($0.01 \leqslant Re \leqslant 40$; $1 \leqslant Pr \leqslant 100$; $0.2 \leqslant n \leqslant 1.8$ and $0.2 \leqslant E \leqslant 5$) can be best represented by the following expression which is of the same form as a recently proposed equation for circular cylinders [15]:

$$Nu = \lambda + F(n) Re^{\alpha} Pr^{\beta} \tag{16}$$

where $F(n) = a^{(-bn+c)} \left(\frac{3n+1}{4n}\right)^{d}$, $\alpha = \frac{e}{fn+1}$ and $\beta = \frac{g}{\ell n+2}$.

The values of the empirically fitted constants (a, b, c, d, e, f, g, ℓ and λ) with their statistical analysis are shown in

Table 7
Variation of the Average Nusselt number (Nu) for heat transfer in non-Newtonian power-law liquids from an unconfined elliptical ($E > 1$) cylinder with Reynolds and Prandtl numbers and power-law index

n	$Re = 0.01$	$Re = 0.1$	$Re = 1$	$Re = 10$	$Re = 40$	$Re = 0.01$	$Re = 0.1$	$Re = 1$	$Re = 10$	$Re = 40$
Pr = 1, E = 2						*Pr = 1, E = 5*				
0.2	0.2275	0.3781	0.8337	2.1386	4.0257	0.1194	0.2149	0.5168	1.3908	2.6963
0.6	0.2261	0.3587	0.6937	1.7714	3.3519	0.1183	0.1990	0.4181	1.1383	2.2177
1	0.2204	0.3398	0.6618	1.6456	3.0024	0.1148	0.1876	0.4007	1.0675	2.0105
1.4	0.2215	0.3447	0.6628	1.5798	2.7900	0.1156	0.1916	0.4047	1.0362	1.8910
1.8	0.2239	0.3508	0.6692	1.5393	2.6504	0.1171	0.1960	0.4115	1.0198	1.8132
Pr = 10, E = 2						*Pr = 10, E = 5*				
0.2	0.3780	0.8340	2.0672	5.4208	10.2948	0.2149	0.5168	1.3457	3.5637	6.8817
0.6	0.3585	0.6723	1.4695	3.9619	7.5669	0.1989	0.3994	0.9233	2.5765	5.0333
1	0.3221	0.5742	1.3087	3.4976	6.4753	0.1757	0.3385	0.8311	2.3176	4.3795
1.4	0.3181	0.5701	1.2763	3.2669	5.9359	0.1742	0.3399	0.8211	2.2035	4.0384
1.8	0.3282	0.5838	1.2733	3.1285	5.6339	0.1811	0.3517	0.8283	2.1409	3.8328
Pr = 50, E = 2						*Pr = 50, E = 5*				
0.2	0.6404	1.5699	3.9137	10.1023	19.0951	0.3895	1.0089	2.5803	6.5827	12.6186
0.6	0.5471	1.1223	2.5327	6.8608	13.0908	0.3188	0.6890	1.6102	4.4747	8.7137
1	0.4499	0.8907	2.1703	5.9223	11.1246	0.2560	0.5456	1.4101	3.9598	7.4760
1.4	0.4296	0.8609	2.0805	5.4644	10.1984	0.2455	0.5353	1.3691	3.7358	6.8564
1.8	0.4419	0.8737	2.0561	5.2001	9.6963	0.2552	0.5500	1.3717	3.6115	6.5227
Pr = 100, E = 2						*Pr = 100, E = 5*				
0.2	0.8339	2.0656	5.1322	13.0948	24.6682	0.5169	1.3451	3.3801	8.4900	16.2254
0.6	0.6717	1.4127	3.2049	8.6759	16.5595	0.3989	0.8752	2.0427	5.6618	11.0099
1	0.5304	1.0917	2.7116	7.4373	14.0406	0.3076	0.6773	1.7638	4.9867	9.4091
1.4	0.4978	1.0438	2.5843	6.8343	12.8818	0.2902	0.6586	1.7126	4.6941	8.6242
1.8	0.5099	1.0547	2.5454	6.5040	12.2722	0.3006	0.6743	1.7121	4.5307	8.2148

Table 8. A comparison between the present numerical results and the predictions of Eq. (16) is shown in Fig. 2. Also, shown in Fig. 2 are the predictions from the expression for average Nusselt number for a circular cylinder ($E = 1$) for power-law fluids [15]. An examination of this table shows that the maximum deviations from Eq. (16) progressively increase as the value of E deviates increasingly from unity. Similarly, further scrutiny of the present numerical results revealed that the points relating to certain combinations of n, Re, Pr or E, especially small values of n

Table 8
Correlation coefficients for the dependence of the average Nusselt number (Nu) and j-factor on the dimensionless parameters (Re, n, Pr and E)

	$E = 0.2$	$E = 0.5$	$E = 1$	$E = 2$	$E = 5$	$E = 0.2$	$E = 0.5$	$E = 1$	$E = 2$	$E = 5$
	Nu					*j-Factor*				
λ	0.7864	0.6717	0.4320	0.2094	0.0864	0.1759	0.1615	0.1324	0.0913	0.0464
a	0.1512	0.1946	0.1102	0.3918	1.6165	0.7946	0.7984	0.7328	0.5940	0.3878
b	−0.0059	−0.0049	−0.0086	0.0286	−0.1651	0.2033	0.2221	0.2400	0.2586	0.2786
c	0.4682	0.4654	0.2857	0.7669	−2.3456	0.5837	0.5592	0.5374	0.5209	0.5085
d	0.4182	0.5135	0.5895	0.6393	0.6362	–	–	–	–	–
e	0.5614	0.5290	0.4762	0.4541	0.4610	–	–	–	–	–
f	−0.0074	−0.0127	−0.0286	−0.0104	0.0150	–	–	–	–	–
g	0.8582	0.8438	0.8151	0.7949	0.7784	–	–	–	–	–
ℓ	0.1674	0.1913	0.2126	0.2379	0.2245	–	–	–	–	–
δ_{max}	47.12	44.44	37.00	24.99	20.99	59.65	57.87	55.31	51.84	45.25
δ_{avg}	9.85	9.11	6.52	4.39	4.25	12.97	11.44	12.74	13.35	12.62
# of data points having large deviations										
$\delta > 40$	6	5	0	0	0	5	5	4	3	3
$\delta > 20$	22	18	8	2	2	26	18	18	14	28
$\delta > 10$	38	32	27	16	16	58	50	74	85	85
After excluding the data points $\delta > 20$										
δ_{max}	17.51	19.40	19.83	18.34	19.36	19.86	19.57	19.85	19.45	19.87
δ_{avg}	4.92	5.09	4.86	4.08	3.98	7.76	7.57	9.55	10.99	10.87

δ: Percent relative r.m.s. deviation from the numerical data (Total # of data points = 120 × 5 = 600).

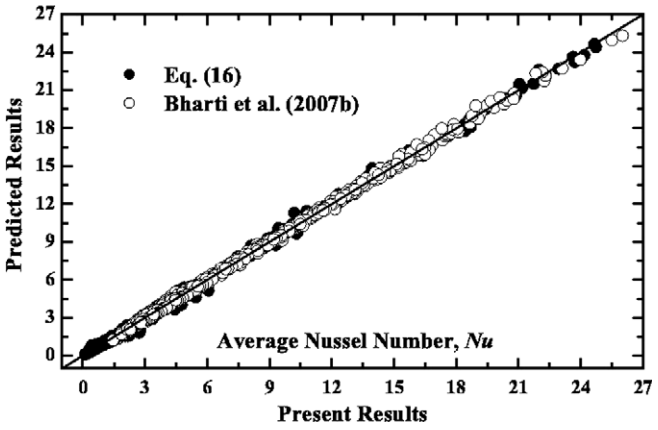

Fig. 2. Comparison of the present average Nusselt number (Nu) results with the prediction of proposed correlations Bharti et al. [15].

and Re, showed rather large deviations. However, if 52 points showing errors larger than 20% are excluded, Eq. (16) reproduces the remaining 548 data points with an average error of 4.8% which rises to a maximum value of 19.8%. In view of the rather wide ranges of parameters covered by Eq. (16), this level of accuracy is regarded to be satisfactory and acceptable, at least for the purpose of process engineering calculations.

6.2.2. Colburn heat transfer factor (j)

In the engineering literature, it is common to use the so-called Colburn j-factor. It is defined as

$$j = \frac{Nu}{RePr^{1/3}}$$

The main virtue of this parameter lies in the fact that it affords the possibility of reconciling the results for a range of Prandtl numbers into a single curve. The variation of the Colburn j-factor with the Reynolds number, power-law index, Prandtl number and the aspect ratio over the range of conditions studied herein is shown in Fig. 3. These figures show qualitatively similar dependence of the Colburn j-factor (to that of circular cylinder, $E = 1$, see middle row of Fig. 3) on the dimensionless parameters (Re, n, Pr, E). For fixed values of the Reynolds and Prandtl numbers and power-law index (n), the value of the j-factor increases from that of a circular cylinder ($E = 1$) (see top three rows of Fig. 3) with the decreasing value of the aspect ratio ($E < 1$), the opposite dependence can be seen (see last three rows of Fig. 3) with the increasing value of the aspect ratio ($E > 1$). For fixed values of the aspect ratio (E) and Prandtl number (Pr), the power-law index (n) has a negligible influence on the j-factor at low Reynolds numbers. Irrespective of the aspect ratio (E) and Prandtl number (Pr), the increasing values of the Reynolds number (Re) show a stronger influence of power-law index (n) on the j-factor in shear-thinning ($n < 1$) fluids than that seen in shear-thickening ($n > 1$) fluids.

Furthermore, the dependence of the Colburn j-factor on the Reynolds number (Re) has been elucidated by plotting the j-factor vs Re on a log–log scale for all values of aspect ratio (E), Prandtl numbers (Pr) and power-law index (n) in Fig. 4. As in the case of Newtonian fluids, the j-factor is seen to vary linearly with the Reynolds number (Re) for all values of aspect ratio (E), Prandtl number (Pr) and power-law index (n). This trend is also consistent with that for circular and square cylinders.

The functional dependence of the present numerical data in terms of the j-factor on the dimensionless parameters (Re, Pr, n, E) over the range of conditions considered here can be best represented by the following expression:

$$j = \frac{\lambda}{Re} + \frac{a}{n^b Re^c} \tag{17}$$

The values of empirically fitted constants (a, b, c, and λ) with their statistical analysis with the present numerical data are shown in Table 8. A comparison between the present numerical results and the predictions of Eq. (17) is shown in Fig. 5. Also, shown in Fig. 5 are the predictions from the expression for j-factor for a circular cylinder ($E = 1$) for power-law fluids [15]. While this approach reconciles data for different values of the Prandtl number, the resulting deviations are somewhat larger than that associated with Eq. (16), as seen in Table 8. The aforementioned errors associated with Eqs. (16) and (17) seem to be rather large, but these results do indeed embrace wide ranges of the pertinent dimensionless parameters. From an engineering standpoint, once again,this level of accuracy is regarded to be acceptable.

6.2.3. Effect of power-law rheology (n)

In order to delineate the role of power-law rheology on heat transfer in an unambiguous manner, the average Nusselt number in power-law fluids has been normalized using the corresponding Newtonian value ($X_N = Nu_n/Nu_{n=1}$ or $= j_n/j_{n=1}$) at the same values of the Reynolds number (Re), Prandtl number (Pr) and the aspect ratio (E). Fig. 6 shows the dependence of X_N on the Reynolds and Prandtl numbers, power-law index and aspect ratio of the elliptical cylinder. These figures show the normalized values to be $X_N > 1$ and $X_N < 1$ for shear-thinning ($n < 1$) and shear-thickening ($n > 1$) fluid behaviours, respectively. It is clearly an indication of heat transfer enhancement in shear-thinning fluids ($n < 1$), while heat transfer shows an opposite dependence (except at low Peclet numbers, $Pe = Re \times Pr$) on the power-law index (n) in shear-thickening ($n > 1$) fluids. Over the range of aspect ratios (E), at low Peclet numbers ($Pe \leqslant 1$), the normalized values (X_N) in shear-thickening fluids are seen to increase from its Newtonian values with the increasing value of power-law index (see first two columns of Fig. 6). While no heat transfer results for power-law fluids are available in the literature for low Reynolds number ($Re < 5$) even for circular cylinder ($E = 1$), the trends reported here are consistent with

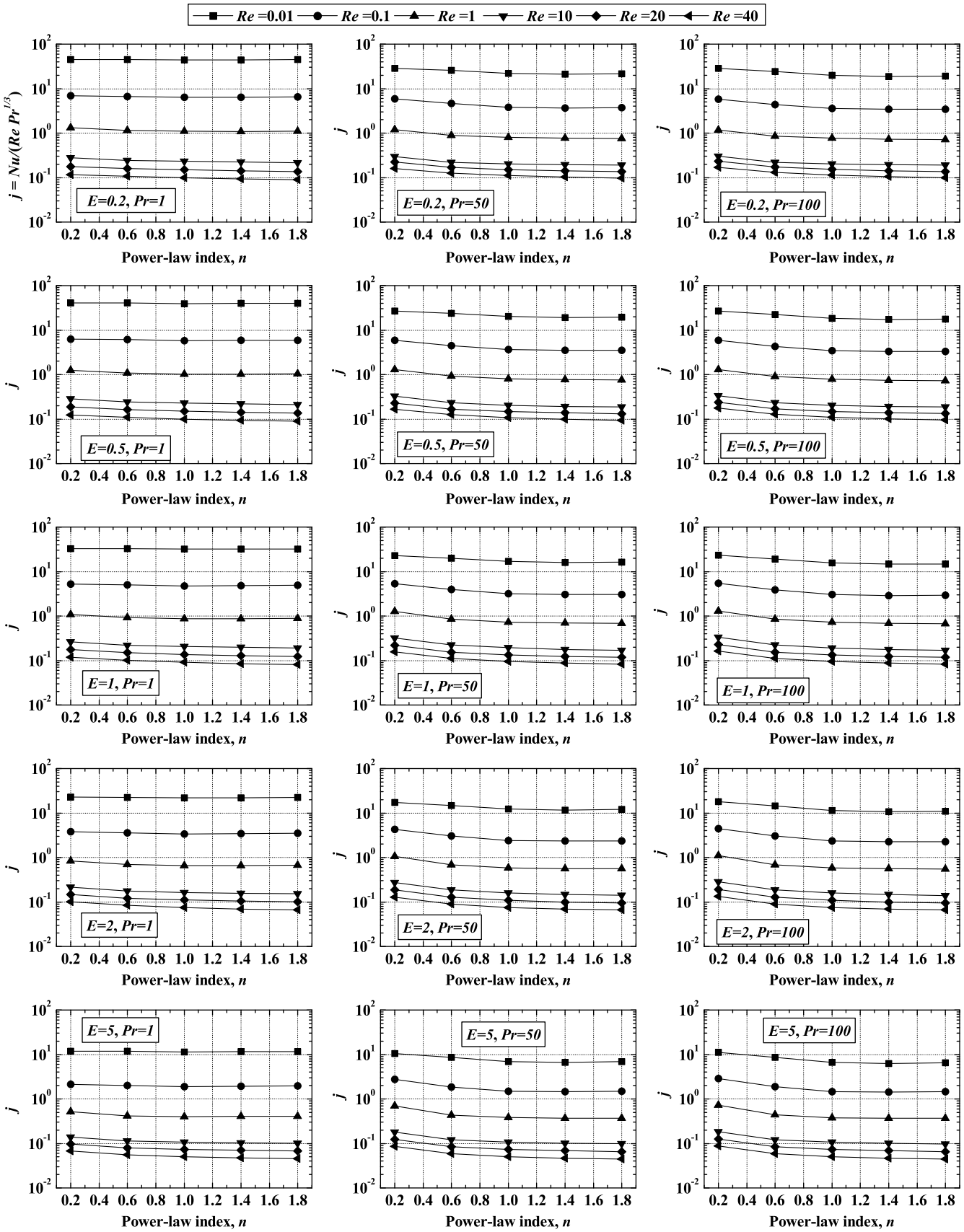

Fig. 3. Dependence of the Colburn heat transfer factor (j) on the Reynolds number (Re), power-law index (n), Prandtl number (Pr) and the aspect ratio (E) of the elliptic cylinder.

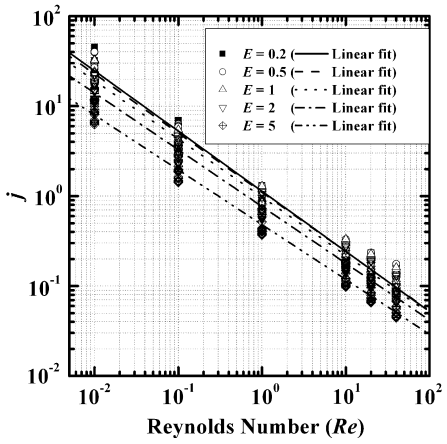

Fig. 4. Colburn heat transfer factor (j) as a function of the Reynolds number at different power-law index, Prandtl number and aspect ratio of the elliptical cylinder.

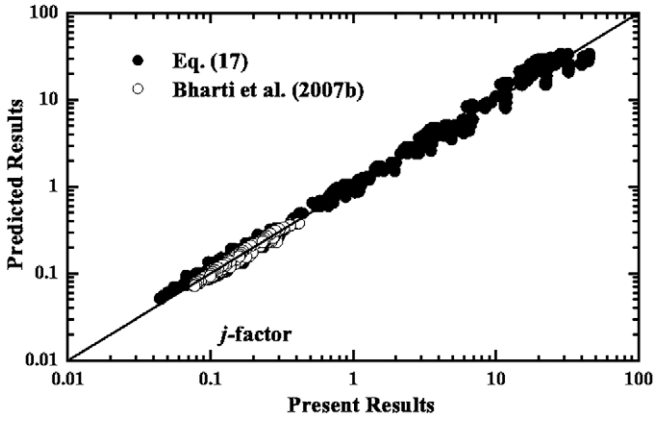

Fig. 5. Comparison of the present j-factor results with the prediction of proposed correlations. Bharti et al. [15].

the literature results for $Re \geqslant 5$ [15,21], the reverse trend seen in shear-thinning fluids is clearly due to very low Peclet numbers ($Pe \leqslant 1$). For fixed values of the Reynolds and Prandtl numbers, power-law index ($n < 1$) and with the decreasing value of the aspect ratio $E < 1$ shows a decrease in the value of X_N, i.e., non-Newtonian effects become weaker (see top three rows of Fig. 6). The opposite dependence of X_N on the power-law index (n) can be seen with the increasing value of E (>1) (see last three rows of Fig. 6). These figures also show a strong effect of flow behaviour index on heat transfer in shear-thinning fluids compared to that in shear-thickening fluids. The normalized values, X_N, can be seen to be as high as two under appropriate conditions in shear-thinning fluids as the value of the power-law index (n) is progressively decreased from 1 to 0.2. On the other hand, the maximum variation in the value of X_N in shear-thickening fluids is seen to be of the order of 15% as the power-law index (n) is varied from 1 to 1.8. The normalized (X_N) values are, however, seen to increase with the increasing aspect ratio (E), while the average Nusselt number (Nu) values show the reverse trend, thereby suggesting a strong interplay between the shape and the power-law rheology.

6.2.4. Effect of shape of the cylinder (E)

In order to delineate the role of shape of the cylinder (E) on heat transfer, the average values of the Nusselt number for elliptical cylinders have been normalized using the corresponding values for a circular cylinder ($X_E = Nu_E/Nu_{E=1}$ or $= j_E/j_{E=1}$) at the same values of the Reynolds number (Re), power-law index (n) and Prandtl number (Pr). Fig. 7 shows the variation of the normalized values (X_E) with the Reynolds and Prandtl numbers, power-law index and aspect ratio of the cylinder. These figures show a rather complex dependence of heat transfer on the shape of the cylinder (E) in conjunction with the kinematic parameters and power-law rheology. For a fixed value of the Prandtl number (Pr), a decrease in the heat transfer ($X_E < 1$) from an elliptic cylinder below that from a circular cylinder ($E = 1$) can be seen with an increase in the value of $E > 1$ (see last two rows of Fig. 7) over the range of power-law index, Reynolds and Prandtl numbers. This seems to suggest the existence of a thicker thermal boundary layer under these conditions. On the other hand, a decrease in the value of the aspect ratio $E < 1$ enhances the heat transfer ($X_E > 1$) from an elliptic cylinder as compared to that from a circular cylinder ($E = 1$) for $E = 0.5$ and for all values of Re, Pr and n (see second row of Fig. 7), however, for $E = 0.2$, the normalized values show a complex dependence on the aspect ratio (E). This clearly suggests a strong interplay between the shape and power-law rheology on heat transfer in this case.

In summary, the average heat transfer coefficient is seen to be influenced in an intricate manner by the values of the Reynolds number (Re), Prandtl number (Pr), the power-law index (n) and the aspect ratio (E). This interplay is further accentuated by the fact that even at low Reynolds numbers, the viscous term in the momentum equations is highly non-linear for power-law fluids. As the Reynolds number is increased, the flow is governed by two non-linear terms, namely, inertial and viscous, which scale differently with velocity. For instance, the viscous forces will approximately scale as $\sim U_\infty^n$ whereas the inertial forces scale as $\sim U_\infty^2$. Thus, keeping everything else fixed, the decreasing value of the power-law index (n) suggests diminishing importance of the viscous effects for shear-thinning ($n < 1$) fluids, while the inertial terms will still scale as $\propto U_\infty^2$. On the other hand, viscous effects are likely to grow with the increasing value of the power-law index (n) for a shear-thickening ($n > 1$) fluid. For the extreme case of $n = 1.8$, the viscous terms will also scale as $\approx U_\infty^{1.8}$, almost identical to the inertial term. These non-linear interactions in conjunction with the shape of the cylinder exert a strong influence on the heat transfer characteristics. It is believed that these different kinds of dependencies on the flow behaviour index and velocity are also responsible for the

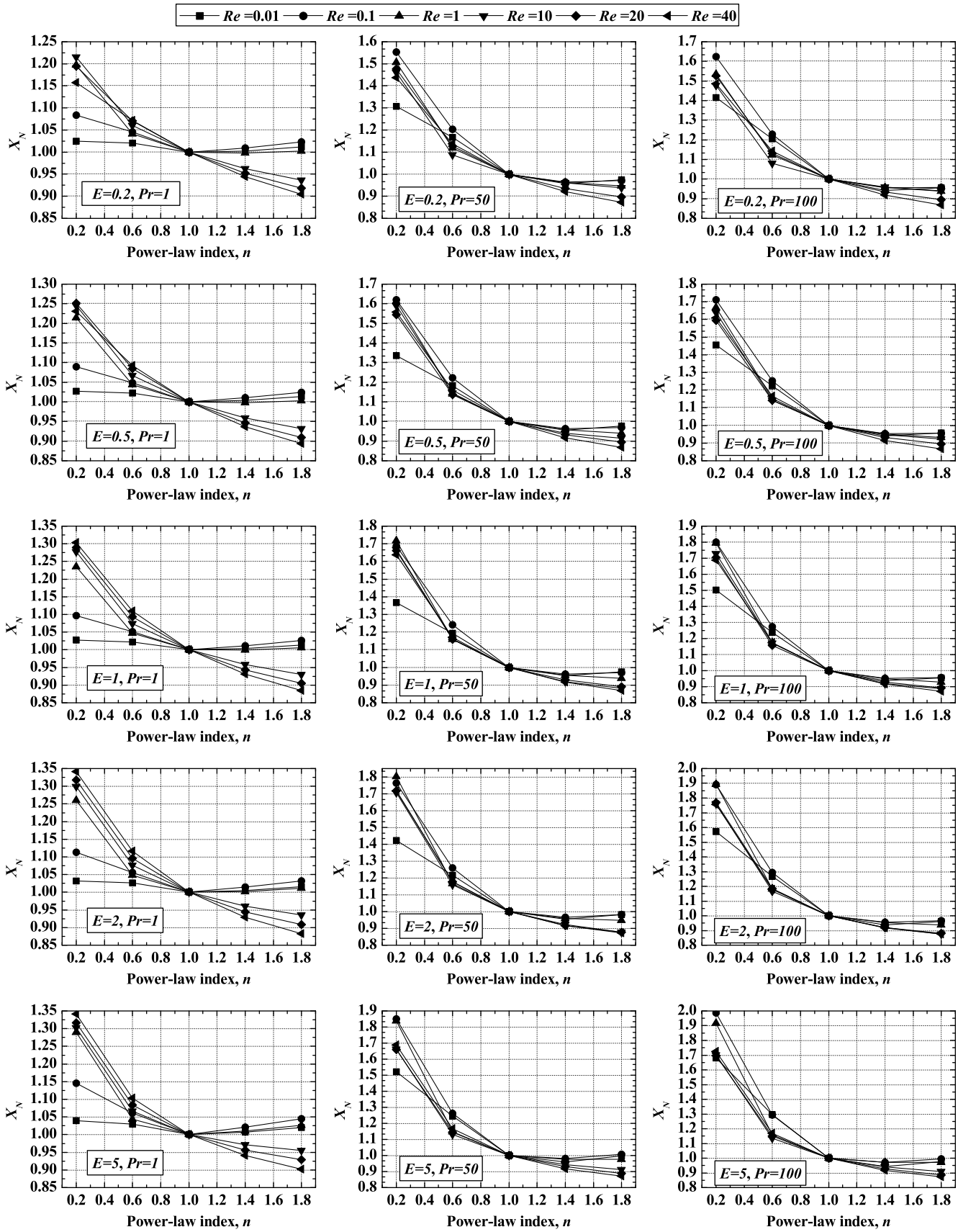

Fig. 6. Dependence of the normalized average Nusselt number and/or j-factor (X_N) on the Reynolds number (Re), power-law index (n), Prandtl number (Pr) and the aspect ratio (E) of the elliptic cylinder.

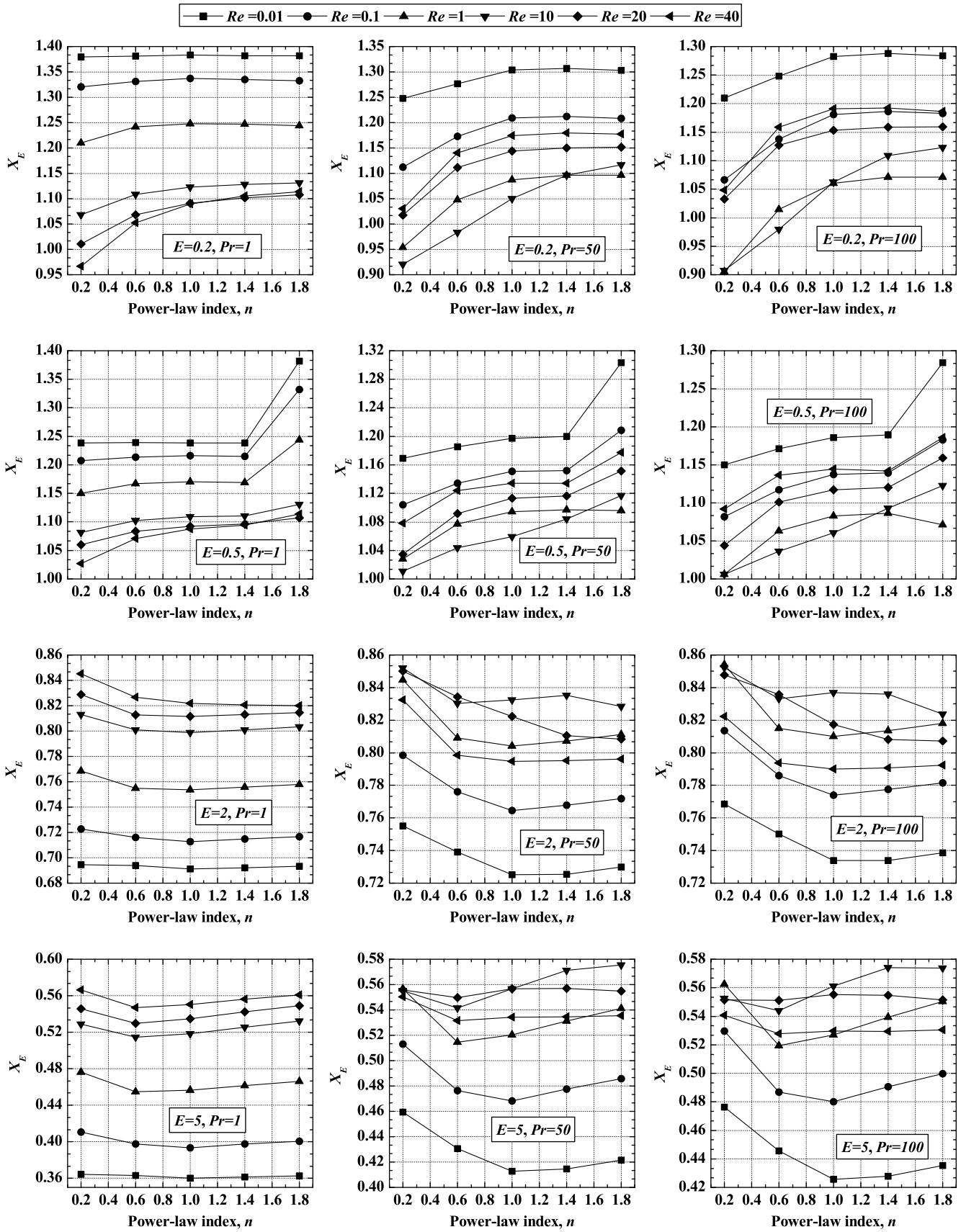

Fig. 7. Dependence of the normalized average Nusselt number and/or *j*-factor (X_E) on the Reynolds number (Re), power-law index (n), Prandtl number (Pr) and the aspect ratio (E) of the elliptic cylinder.

non-monotonic behaviour of flow and heat transfer parameters as seen in this work.

7. Concluding remarks

Extensive numerical results on the average heat transfer from an elliptic cylinder to power-law fluids have been presented over wide ranges of conditions as: $0.01 \leqslant Re \leqslant 40$, $1 \leqslant Pr \leqslant 100$, $0.2 \leqslant n \leqslant 1.8$ and for five values of the aspect ratio ($E = 0.2$, 0.5, 1, 2 and 5). Irrespective of the shape of the cylinder, the average Nusselt number shows a dependence on the Reynolds and Prandtl numbers and power-law index, which is qualitatively similar to that for a circular cylinder. The average heat transfer is facilitated (by up to 100 %) in shear-thinning fluids whereas it is somewhat impeded ($\sim$15%) in shear-thickening fluids. The average Nusselt number values have also been interpreted in terms of the Colburn j-factor. At low Reynolds numbers, the flow behaviour index shows negligible influence on the j-factor. Finally, the functional dependence of the present numerical values on the pertinent dimensionless parameters has also been presented in the form of closure equations which are convenient to use in process engineering calculations.

References

[1] R.A. Ahmad, Steady-state numerical solution of the Navier–Stokes and energy equations around a horizontal cylinder at moderate Reynolds numbers from 100 to 500, Heat Transfer Eng. 17 (1996) 31–81.

[2] R.P. Chhabra, Hydrodynamics of non-spherical particles in non-Newtonian fluids, in: N.P. Cheremisinoff, P.N. Cheremisinoff (Eds.), Handbook of Applied Polymer Processing Technology, Marcel Dekker, New York, NY, 1996 (Chapter 1).

[3] R.P. Chhabra, Heat and mass transfer in rheologically complex systems, in: D. Siginer, D. De Kee, R.P. Chhabra (Eds.), Advances in the Rheology and Flow of Non-Newtonian Fluids, Elsevier, Amsterdan, 1999 (Chapter 39).

[4] R.P. Chhabra, Bubbles, Drops and Particles in Non-Newtonian Fluids, second ed., CRC Press, Boca Raton, FL, 2006.

[5] M.M. Zdravkovich, Flow around Circular Cylinders. Vol. 1: Fundamentals, Oxford University Press, New York, USA, 1997.

[6] M.M. Zdravkovich, Flow around Circular Cylinders. Vol. 2: Applications, Oxford University Press, New York, USA, 2003.

[7] R.P. Chhabra, J.F. Richardson, Non-Newtonian Flow in Process Industries: Fundamentals and Engineering Applications, Butterworth-Heinemann, Oxford, 1999.

[8] R.P. Bharti, R.P. Chhabra, V. Eswaran, A numerical study of the steady forced convection heat transfer from an unconfined circular cylinder, Heat Mass Transfer 43 (2007) 639–648.

[9] P. Sivakumar, R.P. Bharti, R.P. Chhabra, Steady flow of power-law fluids across an unconfined elliptical cylinder, Chem. Eng. Sci. 62 (2007) 1682–1702.

[10] J.M. Ferreira, R.P. Chhabra, Analytical study of drag and mass transfer in creeping power-law flow across a tube bank, Ind. Eng. Chem. Res. 43 (2004) 3439–3450.

[11] E. Marusic-Paloka, On the Stokes paradox for power-law fluids, Z. Angew. Math. Mech. 81 (2001) 31–36.

[12] R.I. Tanner, Stokes paradox for power-law fluids around a cylinder, J. Non-Newtonian Fluid Mech. 50 (1993) 217–224.

[13] M.J. Whitney, G.J. Rodin, Force–velocity relationships for rigid bodies translating through unbounded shear-thinning power-law fluids, Int. J. Non-Linear Mech. 34 (2001) 947–953.

[14] R.P. Bharti, R.P. Chhabra, V. Eswaran, Steady flow of power-law fluids across a circular cylinder, Can. J. Chem. Eng. 84 (2006) 406–421.

[15] R.P. Bharti, R.P. Chhabra, V. Eswaran, Steady forced convection heat transfer from a heated circular cylinder to power-law fluids, Int. J. Heat Mass Transfer 50 (2007) 977–990.

[16] R.P. Bharti, R.P. Chhabra, V. Eswaran, Two-dimensional steady Poiseuille flow of power-law fluids across a circular cylinder in a plane confined channel: wall effects and drag coefficients, Ind. Eng. Chem. Res. 46 (2007) 3820–3840.

[17] R.P. Bharti, R.P. Chhabra, V. Eswaran, Effect of blockage on heat transfer from a cylinder to power law liquids, Chem. Eng. Sci. 62 (2007) 4729–4741.

[18] R.P. Chhabra, A.A. Soares, J.M. Ferreira, Steady non-Newtonian flow past a circular cylinder: a numerical study, Acta Mech. 172 (2004) 1–16.

[19] S.J.D. D'Alessio, L.A. Finlay, Power-law flow past a cylinder at large distances, Ind. Eng. Chem. Res. 43 (2004) 8407–8410.

[20] S.J.D. D'Alessio, J.P. Pascal, Steady flow of a power-law fluid past a cylinder, Acta Mech. 117 (1996) 87–100.

[21] P. Sivakumar, R.P. Bharti, R.P. Chhabra, Effect of power-law index on critical parameters for power-law flow across an unconfined circular cylinder, Chem. Eng. Sci. 61 (2006) 6035–6046.

[22] P. Sivakumar, R.P. Bharti, R.P. Chhabra, Steady power-law flow over a circular cylinder. Recent Advances in Computational Mechanics and Simulations, in: D. Maity, S.K. Dwivedy (Eds.), Proceedings of the Second International Congress on Computational Mechanics and Simulations (ICCMS-06), vol. II, IIT Guwahati, India, 2006, pp. 1254–1260. December 8–10, Paper No. 170.

[23] A.A. Soares, J.M. Ferreira, R.P. Chhabra, Flow and forced convection heat transfer in cross flow of non-Newtonian fluids over a circular cylinder, Ind. Eng. Chem. Res. 44 (2005) 5815–5827.

[24] U.K. Ghosh, S.N. Upadhyay, R.P. Chhabra, Heat and mass transfer from immersed bodies to non-Newtonian fluids, Adv. Heat Transfer 25 (1994) 251–319.

[25] J.K. Woods, P.D.M. Spelt, P.D. Lee, T. Selerland, C.J. Lawrence, Creeping flows of power-law fluids through periodic arrays of elliptical cylinders, J. Non-Newtonian Fluid Mech. 111 (2003) 211–228.

[26] B. Chao, R. Fagbenle, On Merk's methods of calculating boundary layer transfer, Int. J. Heat Mass Transfer 17 (1974) 223–240.

[27] W.A. Khan, J.R. Culham, M.M. Yovanovich, Fluid flow around and heat transfer from elliptical cylinders: analytical approach, J. Thermophys. Heat Transfer 19 (2005) 178–185.

[28] S.J.D. D'Alessio, S.C.R. Dennis, Steady laminar forced convection from an elliptic cylinder, J. Eng. Math. 29 (1995) 181–193.

[29] H.M. Badr, Mixed convection from a straight isothermal tube of elliptic cross-section, Int. J. Heat Mass Transfer 37 (1994) 2343–2365.

[30] H.M. Badr, Forced convection from a straight elliptical tube, Heat Mass Transfer 34 (1998) 229–236.

[31] E.H. Ahmad, H.M. Badr, Mixed convection from an elliptic tube placed in a fluctuating free stream, Int. J. Eng. Sci. 39 (2001) 669–693.

[32] U.R. Ilgrabuis, A. Butkus, Hydraulic drag and average heat transfer coefficients of compact bundles of elliptical finned tubes, Heat Transfer Soviet Res. 20 (1988) 12–21.

[33] H. Nishiyama, T. Ota, T. Matsuno, Forced convection heat transfer from two elliptic cylinders in a tandem arrangement, Trans. JSME B 52 (1986) 2677–2681.

[34] H. Nishiyama, T. Ota, T. Matsuno, Heat transfer and flow around elliptical cylinders in a tandem arrangement, JSME Int. J. Ser. II 31 (1988) 410–419.

[35] S.C.R. Dennis, P.J.S. Young, Steady flow past an elliptic cylinder inclined to the stream, J. Eng. Math. 47 (2003) 101–120.

[36] S.A. Johnson, M.C. Thompson, K. Hourigan, Flow past elliptical cylinder at low Reynolds numbers, in: Proceedings of 14th Austral-

asian Fluid Mechanics Conference, Adelaide University, 9–14 December, 2001, pp. 343–346.
[37] S.A. Johnson, M.C. Thompson, K. Hourigan, Predicted low frequency structures in the wake of elliptical cylinders, Eur. J. Mech. B/Fluids 23 (2004) 229–239.
[38] H.J. Lugt, H.J. Haussling, Laminar flow past an abruptly accelerated elliptic cylinder at 45° incidence, J. Fluid Mech. 65 (1974) 711–734.
[39] J.K. Park, S.O. Park, J.M. Hyun, Flow regimes of unsteady laminar flow past a slender elliptic cylinder at incidence, Int. J. Heat Fluid Flow 10 (1989) 311–317.
[40] S.C.R. Dennis, J.D. Hudson, N. Smith, Steady laminar forced convection from a circular cylinder at low Reynolds numbers, Phys. Fluids 11 (1968) 933–940.
[41] C.F. Lange, F. Durst, M. Breuer, Momentum and heat transfer from cylinders in laminar cross flow at $10^{-4} \leqslant Re \leqslant 200$, Int. J. Heat Mass Transfer 41 (1998) 3409–3430.
[42] S. Mettu, N. Verma, R.P. Chhabra, Momentum and heat transfer from an asymmetrically confined circular cylinder in a plane channel, Heat Mass Transfer 42 (2006) 1037–1048.